Supporting Information

Conversion-Alloying Electrodes for Lithium-ion Batteries: Entropy and Nano-Level Heterogeneity Effects

*Sajid Alvi, Andrea Fazi, Daniel Weber, Daniel Hedman, Kriti Choudhary, Olof Bäcke, Farid Akhtar, Jean-Noel Chotard, Mattias Thuvander, and Patrik Johansson**

Table S1. Elemental masses (g) used to synthesize the metal tellurides.

Comp./ Elements	Sn	Sb	Bi	Ge	Zn	Cu	Te
ST		1.9440					3.0559
GT				1.8138			3.1861
SSBT	0.7118	0.7301	1.2531				2.3047
SSGT	0.8529	0.8748		0.5219			2.7503
SSBT-Ge	0.5748	0.5896	1.0120	0.3517			2.4716
SSBT-Zn	0.5789	0.5938	1.0191		0.3188		2.4891
SSBT-GeCu	0.4850	0.4975	0.8539	0.2968		0.2596	2.6069

Table S2. Calculations of theoretical capacities and the resulting current densities used for the C/5 rate cycling for the synthesized metal tellurides.

Comp./ Elements	Sn	Sb	Bi	Ge	Zn	Cu	Te	Total Capacity mAh g^{-1}	mA g^{-1} for C/5
ST		0.4*660					0.6*420	516	103
GT				0.5*1623			0.5*420	1021.5	202
SSBT	0.1667*990	0.1667*660	0.1667*385				0.5*420	549.2	100
SSGT	0.1667*990	0.1667*660		0.1667*1623			0.5*420	755.5	126
SSBT-Ge	0.125*990	0.125*660	0.125*385	0.125*1623			0.5*420	667.3	107
SSBT-Zn	0.125*990	0.125*660	0.125*385		0.125*385		0.5*420	515.6	103
SSBT-GeCu	0.1*990	0.1*660	0.1*385	0.1*1623		0.1*0	0.5*420	575.8	100

Table S3. Lattice parameters from Pawley's refinements for the synthesized metal tellurides.

Comp.	ΔS	ε_o (%)	GoF	P-1	SG-1	Lattice parameters (Å)		P-2	SG-2	Lattice Parameters		
						a = b	c			a	b	c
GT	0.6 R	0.376 (9)	1.06	GeTe	R3mH	4.161 (8)	10.508 (17)					
ST	0.6 R	0.0387 (4)	1.07	Sb_2Te_3	R-3mH	4.262 (3)	30.368 (6)					
SSBT	1.16 R	0.512 (11)	1.16	$Sn_{1/6}Sb_{1/6}Bi_{1/6}Te_{1/2}$	R-3mH	4.375 (6)	29.079 (9)					
SSBT (SPS)	1.16 R	0.194 (2)	1.33	$Sn_{1/6}Sb_{1/6}Bi_{1/6}Te_{1/2}$	R-3mH	4.369 (3)	29.571 (29)					
SSGT	1.16 R	0.393 (3)	1.14	$Sn_{1/6}Sb_{1/6}Bi_{1/6}Te_{1/2}$	R3mH	4.325 (7)	10.657 (3)					
SSBT-Ge	1.38 R	0.50 (2)	1.01	$Sn_{1/8}Sb_{1/8}Bi_{1/8}Ge_{1/8}Te_{1/2}$	R-3mH	4.590 (2)	28.452 (19)	GeO_2	P42/mnm	4.359 (2)	4.359 (2)	2.891 (6)
SSBT-Ge (SPS)	1.38 R	0.214 (1)	1.3	$Sn_{1/8}Sb_{1/8}Bi_{1/8}Ge_{1/8}Te_{1/2}$	R-3mH	4.613 (5)	28.543 (6)	GeO_2	P42/mnm	4.377 (7)	4.377 (7)	2.9075 (9)
SSBT-Zn	1.38 R	2.93	1.55	$Sn_{1/8}Sb_{1/8}Bi_{1/8}Zn_{1/8}Te_{1/2}$	R-3mH	4.625 (11)	28.573 (16)	ZnTe	F4-3m	6.160 (3)	6.160 (3)	6.160 (3)
SSBT-GeCu	1.61 R	0.31 (5)	1.05	$Sn_{1/12}Sb_{1/12}Bi_{1/12}Ge_{1/12}Cu_{1/12}Te_{1/2}$	R-3mH	4.316 (8)	28.300 (17)	$Cu_{1.75}Te$	P-3m1	8.336	8.336	7.196

Symbols: εo = microstrain; Comp. = compositions; GoF = Goodness of fit; P = Phase; SG = Space group

Table S4. Elemental compositions (at. %) of synthesized metal tellurides from EDX point analysis.

Comp./ Elements	Sn	Sb	Bi	Ge	Zn	Cu	Te
ST		41 ± 0.3					59 ± 0.3
GT				65 ± 3			35 ± 3
SSBT	17 ± 0.3	17 ± 0.3	16 ± 2				50 ± 1
SSGT	17 ± 0.5	17 ± 0.7		18 ± 3			48 ± 2
SSBT-Ge	12 ± 0.2	11 ± 0.2	15 ± 0.3	19 ± 1			43 ± 0.4
SSBT-Zn	13 ± 0.2	12 ± 0.2	13 ± 0.2		16 ± 1		47 ± 0.5
SSBT-GeCu	10 ± 0.3	10 ± 0.3	9 ± 0.3	11 ± 2		13 ± 2	47 ± 1

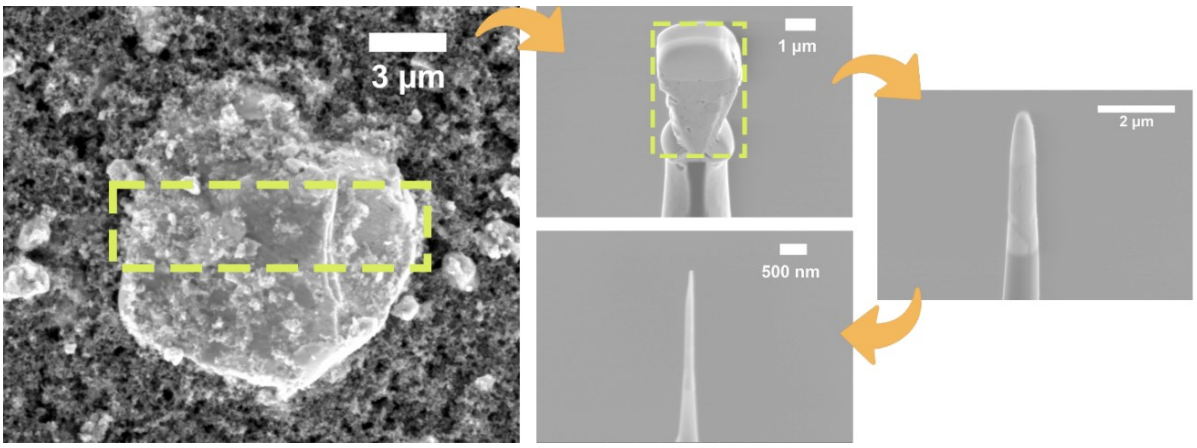

Fig. S1. FIB lift-out procedure from an active material (metal telluride) embedded in the coated electrode.

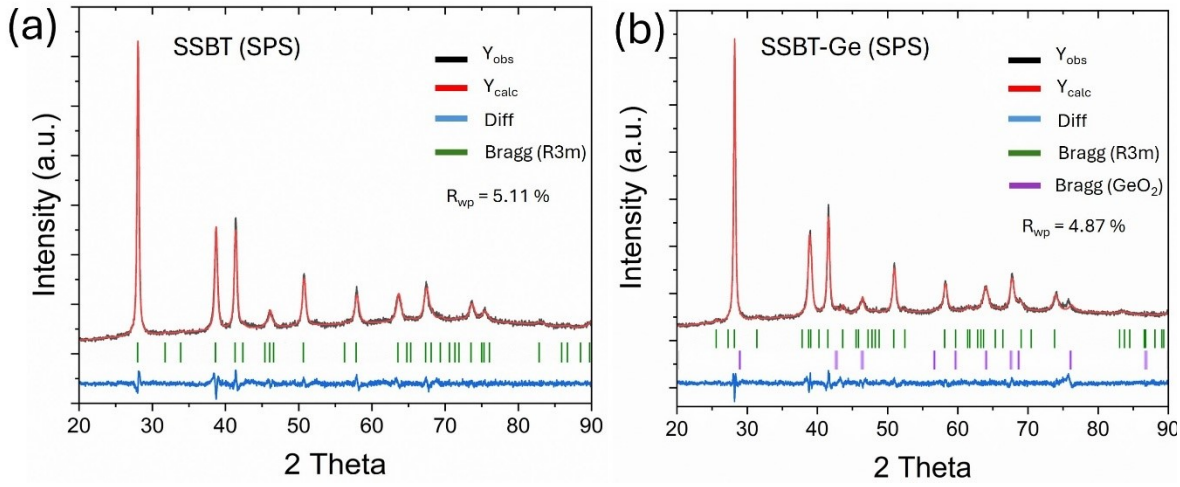

Fig. S2. X-ray diffractograms of ball milled: a) SSBT and b) SSBT-Ge, both after SPS.

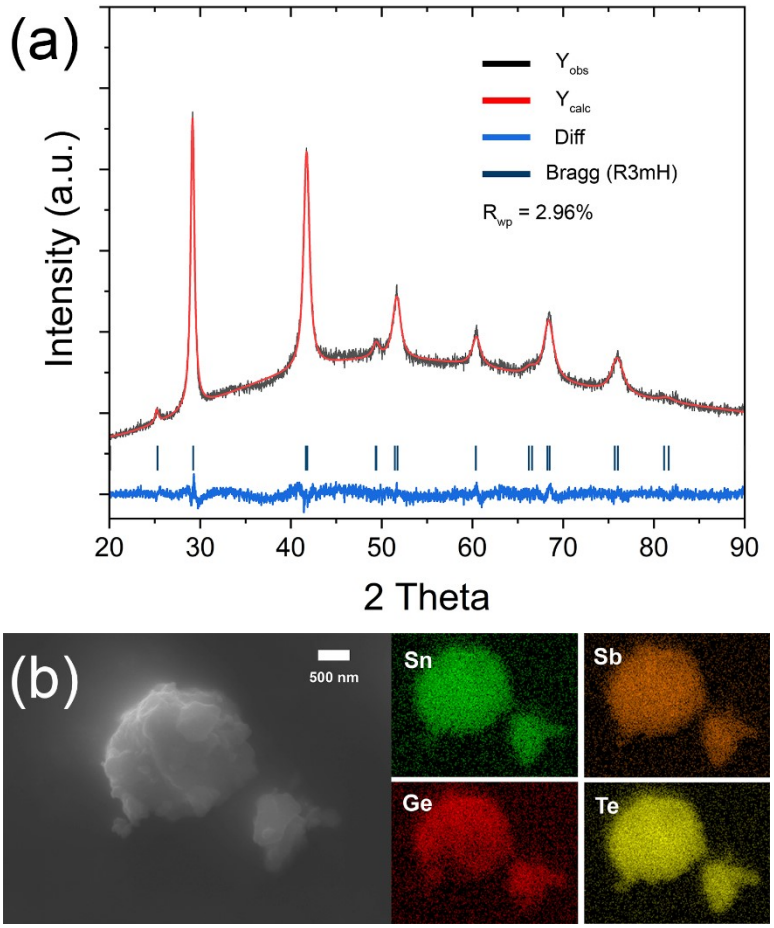

Fig. S3. a) X-ray diffractogram and b) SEM-EDS mapping of SSGT.

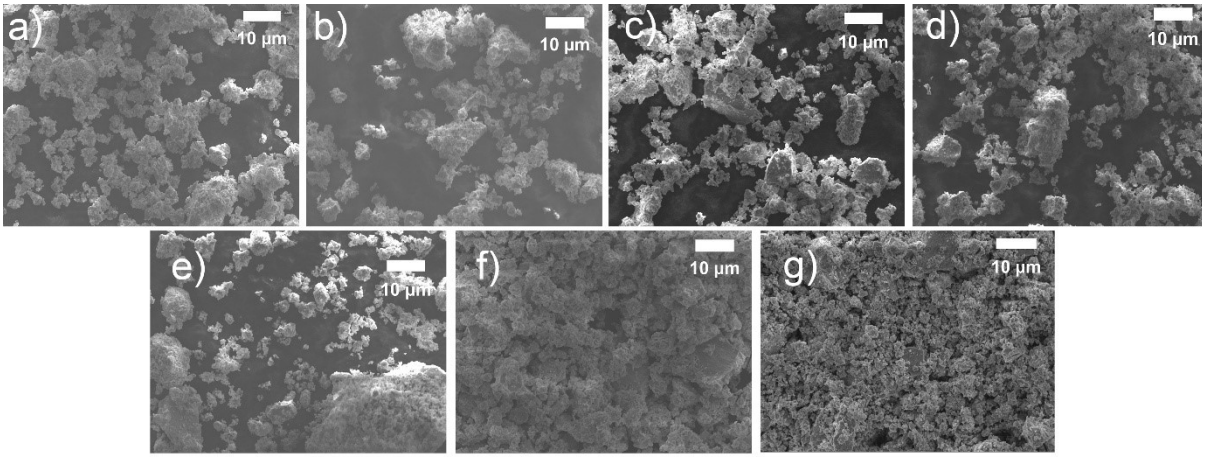

Fig. S4. SEM of as-prepared powders of: a) ST, b) GT, c) SSBT, d) SSGT, e) SSBT-Ge, f) SSBT-Zn, and g) SSBT-GeCu.

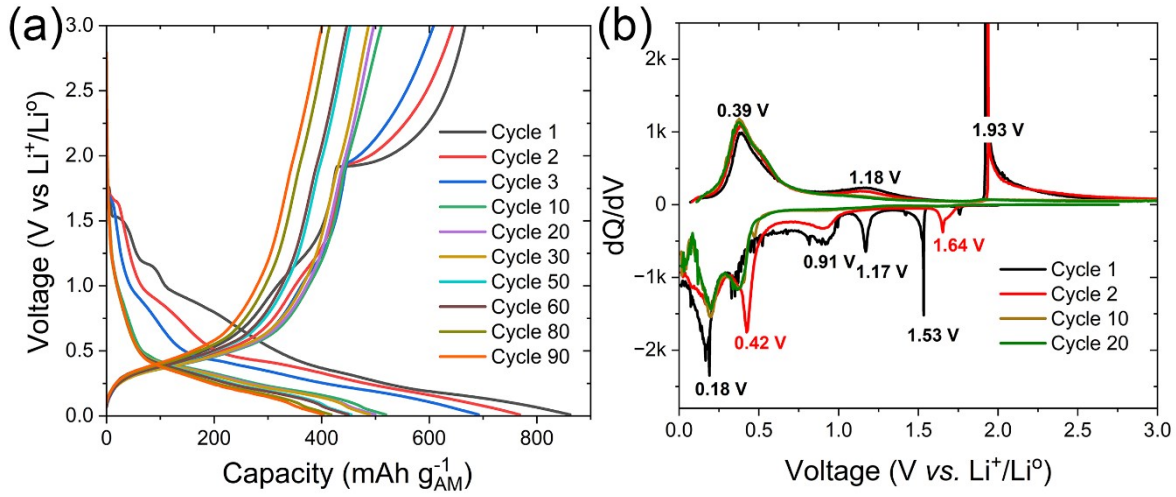

Fig. S5. a) charge-discharge curves and b) $dQdV^{-1}$ of GT in lithium half-cells.

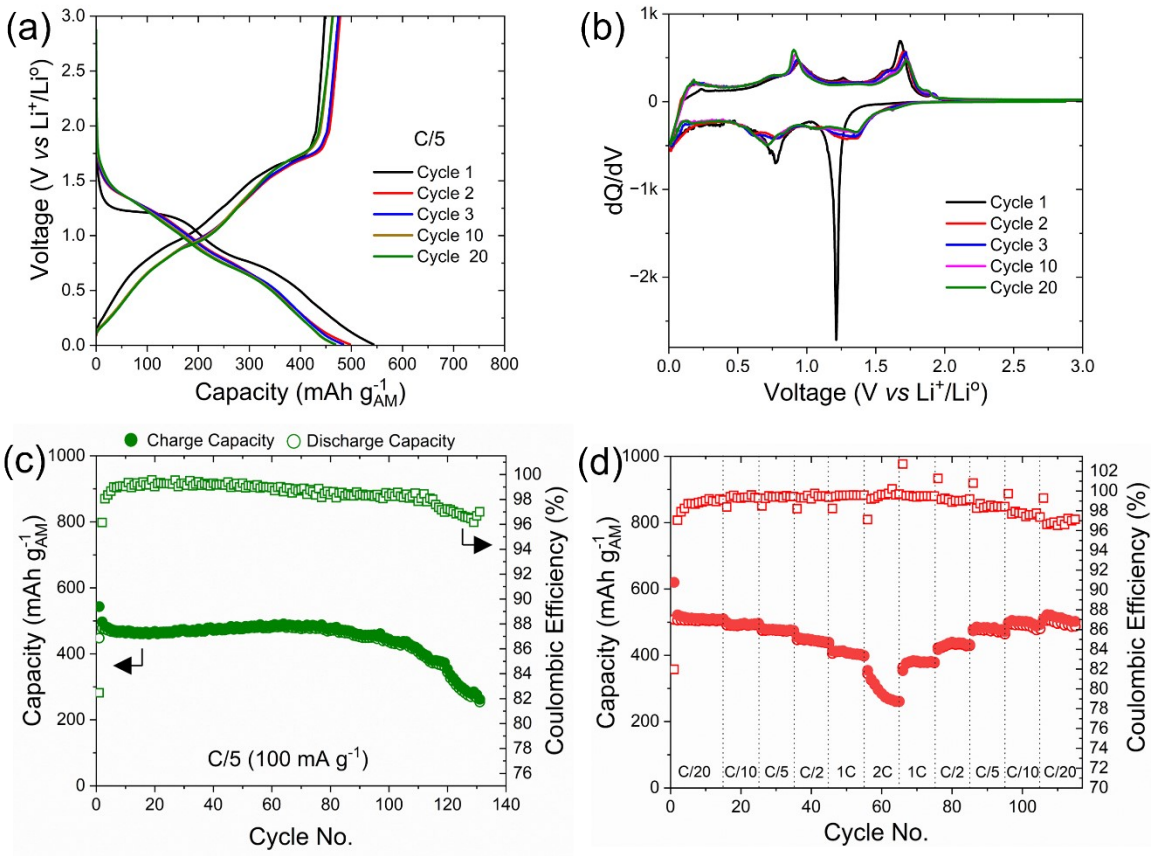

Fig. S6. a) charge-discharge curves, b) dQ dV^{-1}, c) galvanostatic cycling, and d) rate performance of SSBT-Zn.

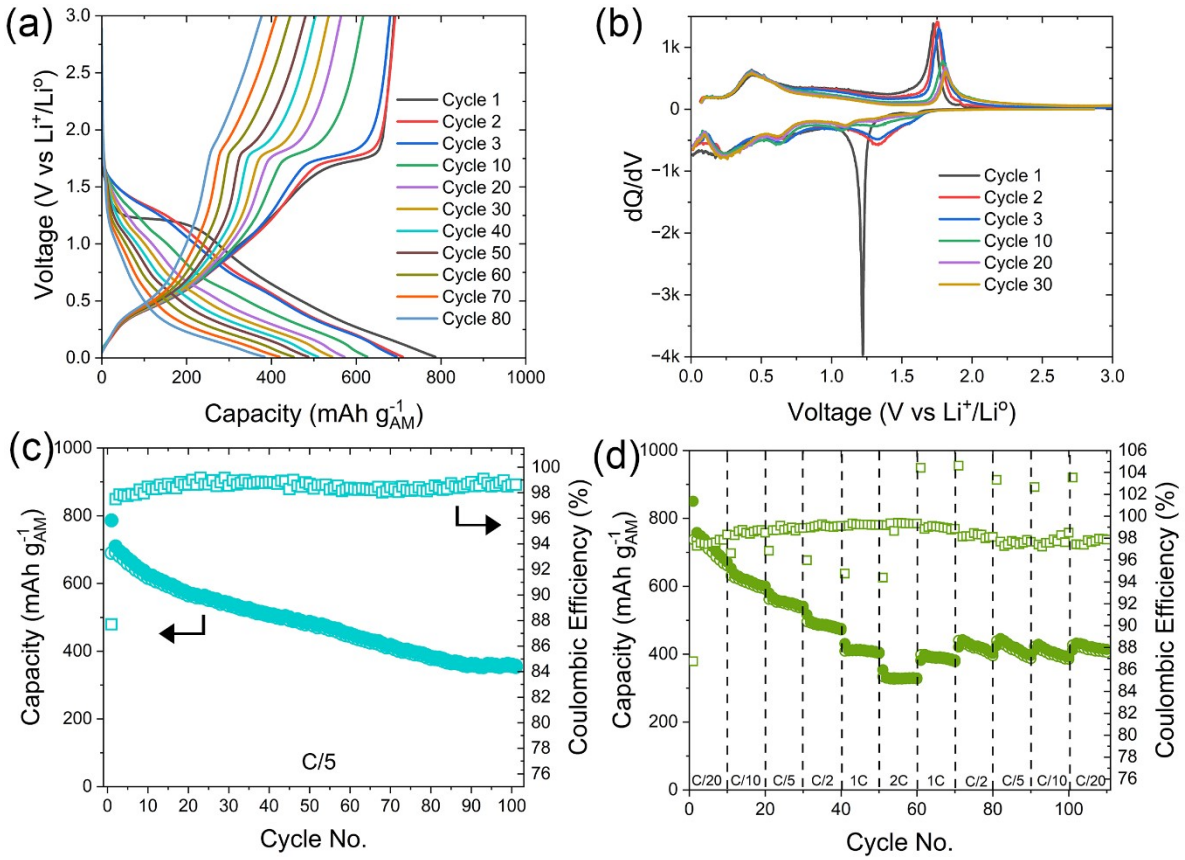

Fig. S7. a) charge-discharge curves, b) dQ dV^{-1}, c) galvanostatic cycling, and d) rate performance of SSGT in half-cells. (Symbols in (c) and (d): closed circle is discharge capacity, open circle is charge capacity, and open rectangle is CE)

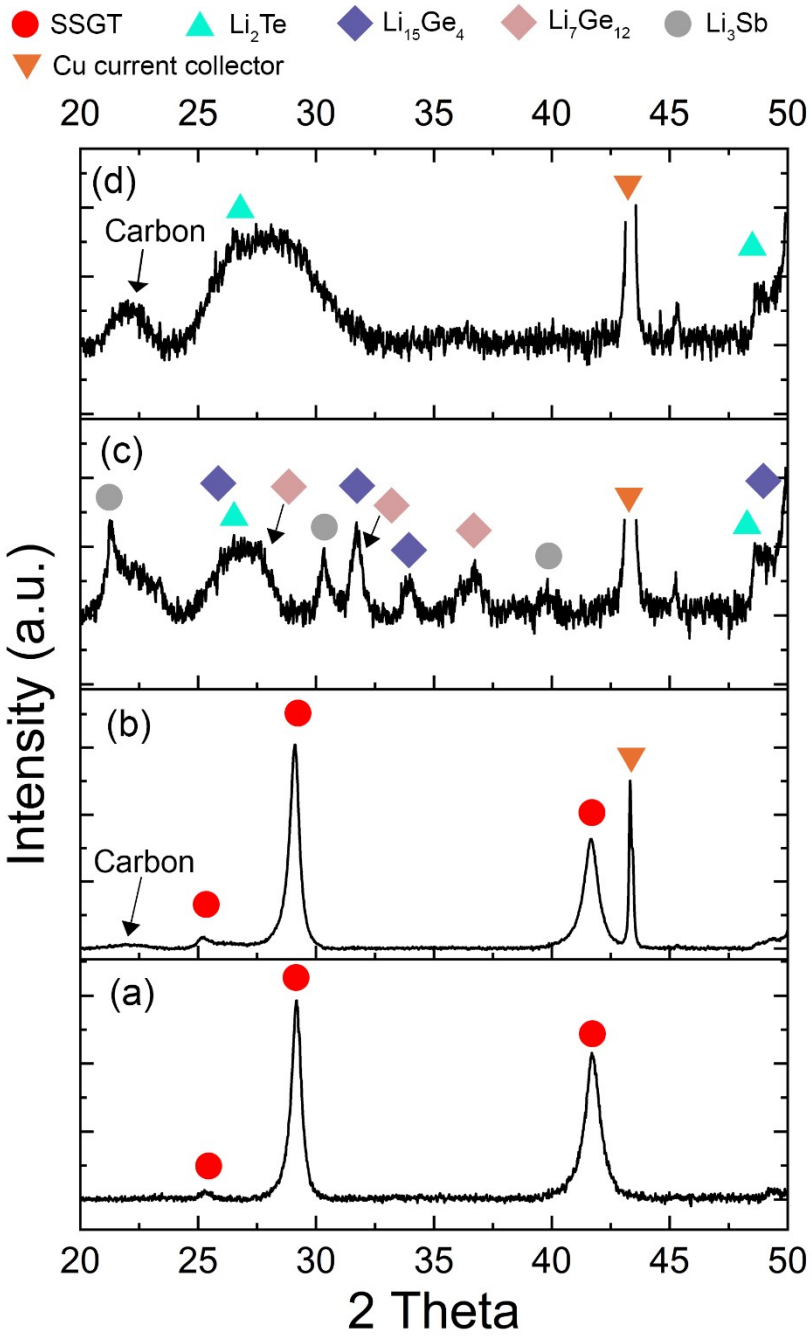

Fig. S8. XRD of a) as-synthesized powder, b) fresh electrode, c)fully lithiated electrode, and d) 1 cycled electrode of SSGT.

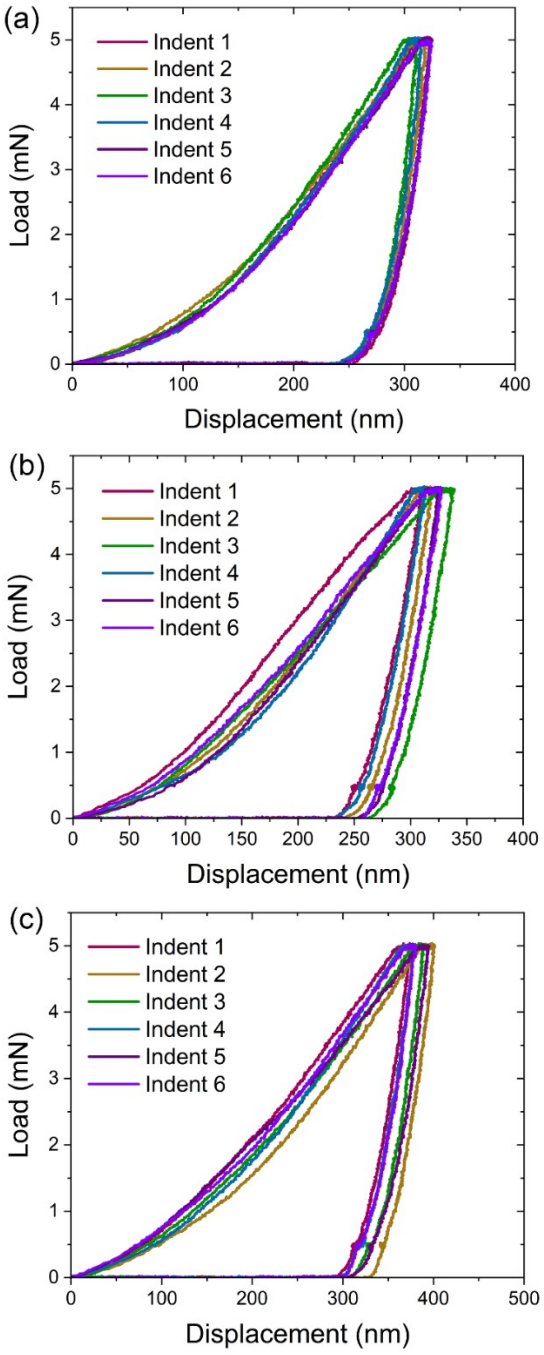

Fig. S9. Nanoindentation for sintered pellets of: a) ST, b) SSBT, and c) SSBT-Ge.

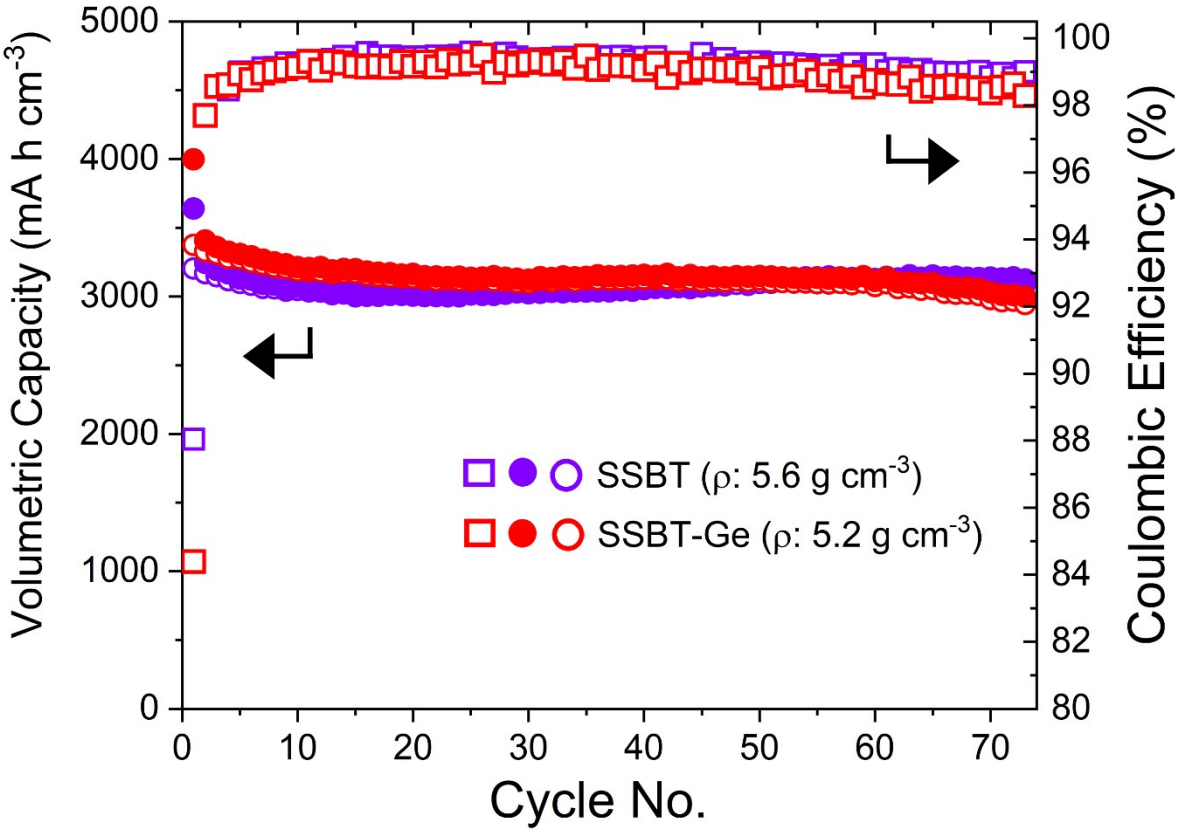

Fig. S10. Galvanostatic cycling of SSBT and SSBT-Ge.

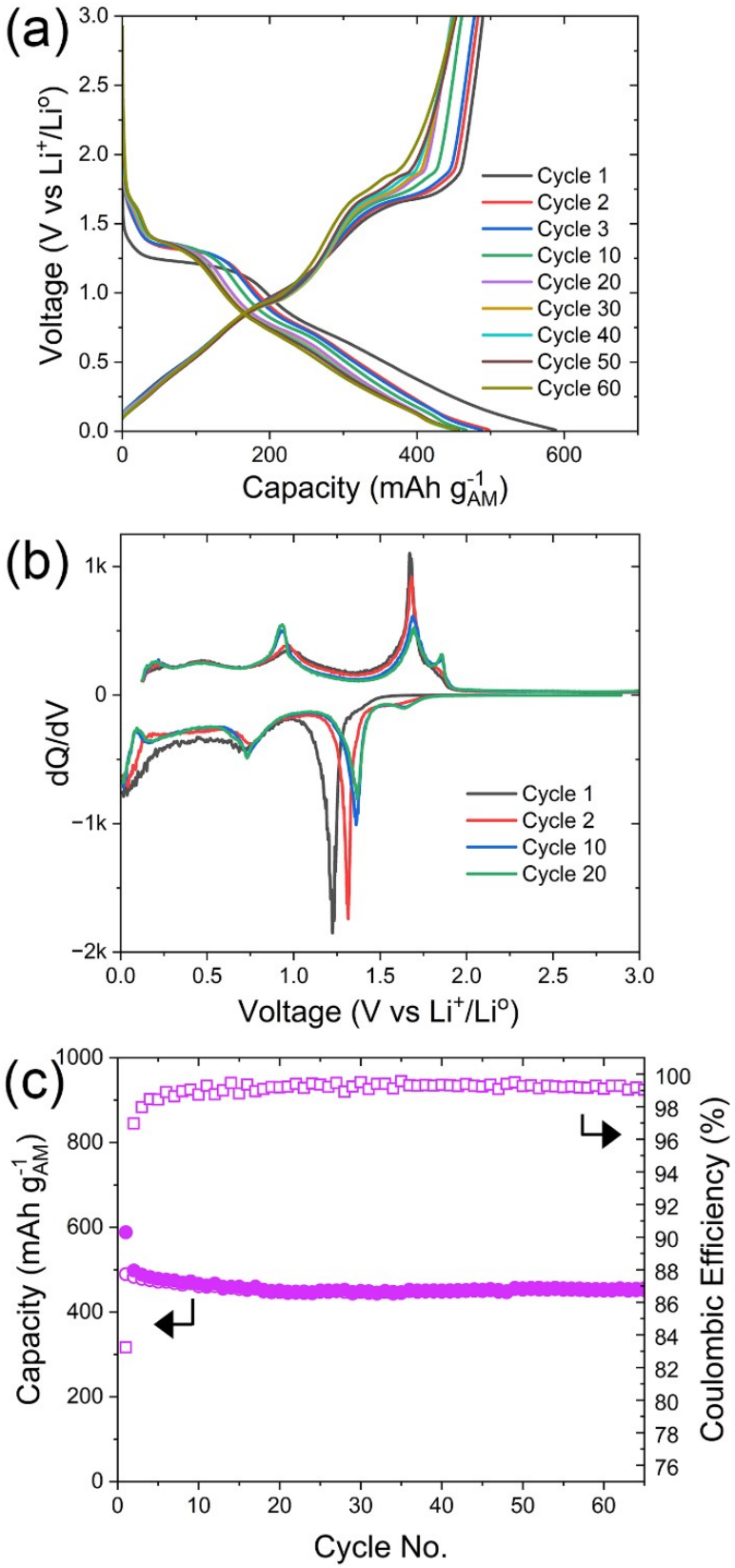

Fig. S11. a) charge-discharge curves, b) dQ dV^{-1}, and c) galvanostatic cycling of SSBT-GeCu with more lean electrolyte (30 µl) cells at C/5 rate.

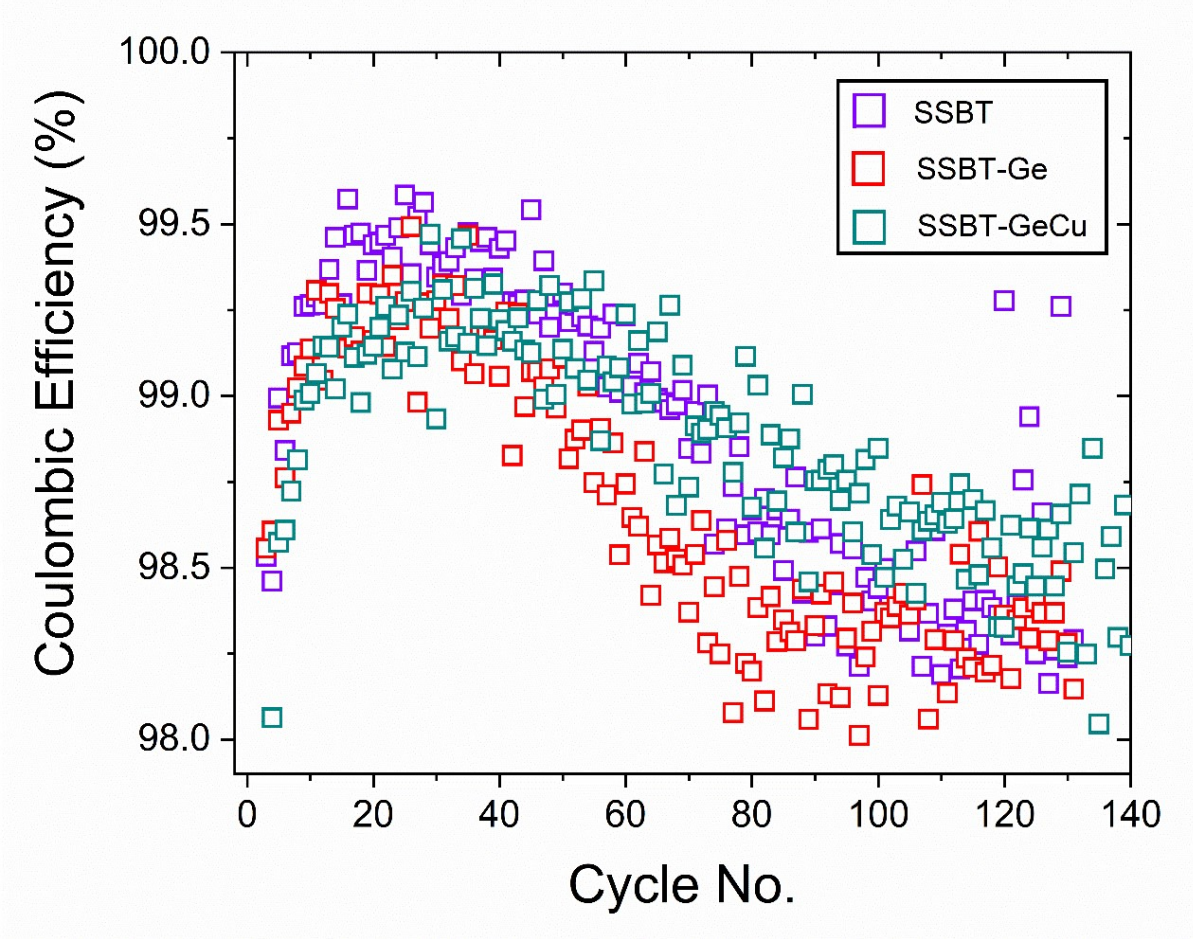

Fig. S12. Coulombic efficiency of SSBT, SSBT-Ge, and SSBT-GeCu for 140 cycles at C/5 in lithium half-cells

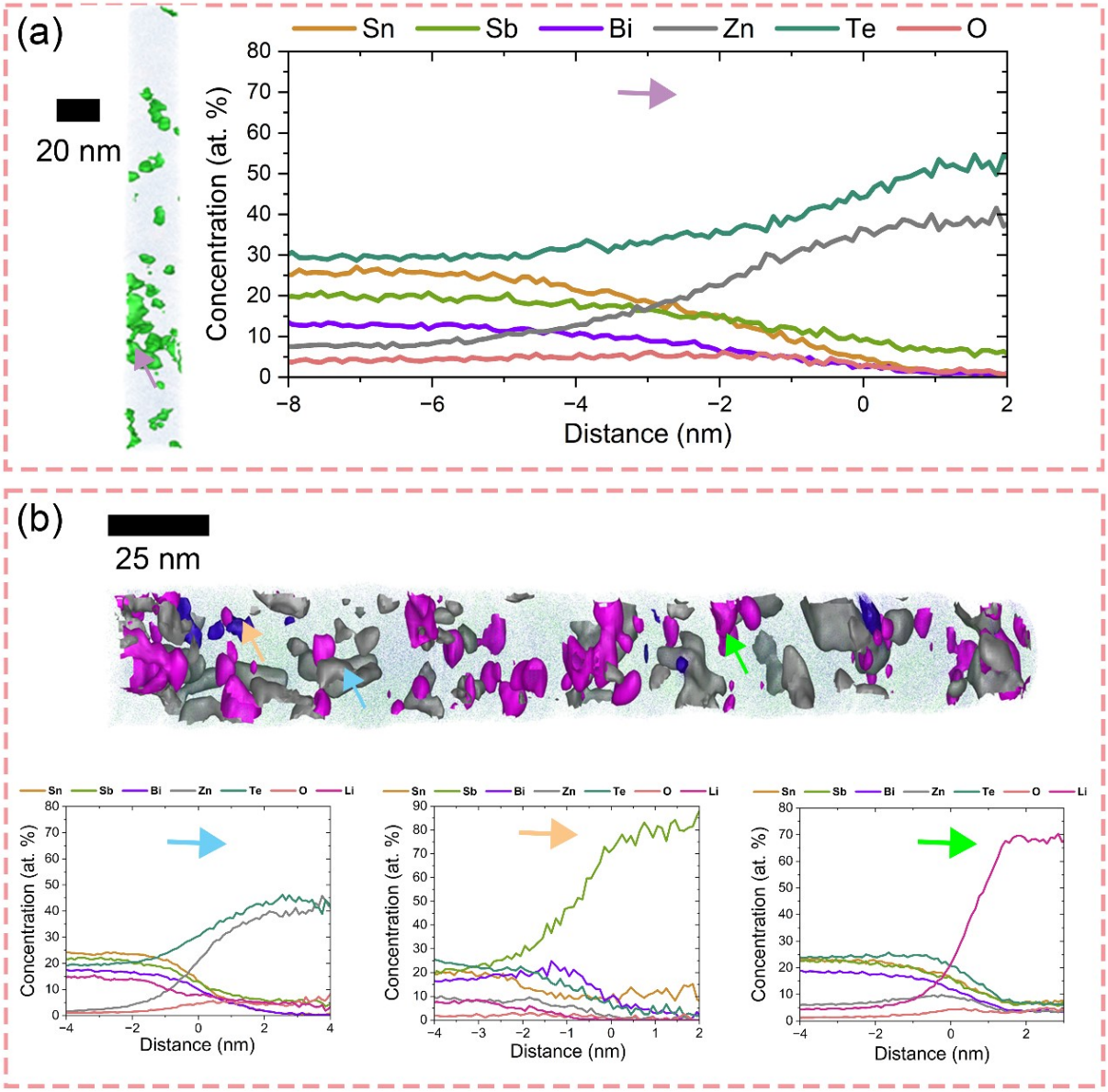

Fig. S13. APT of SSBT-Zn from: a) fresh electrode, and b) after 3 cycles.

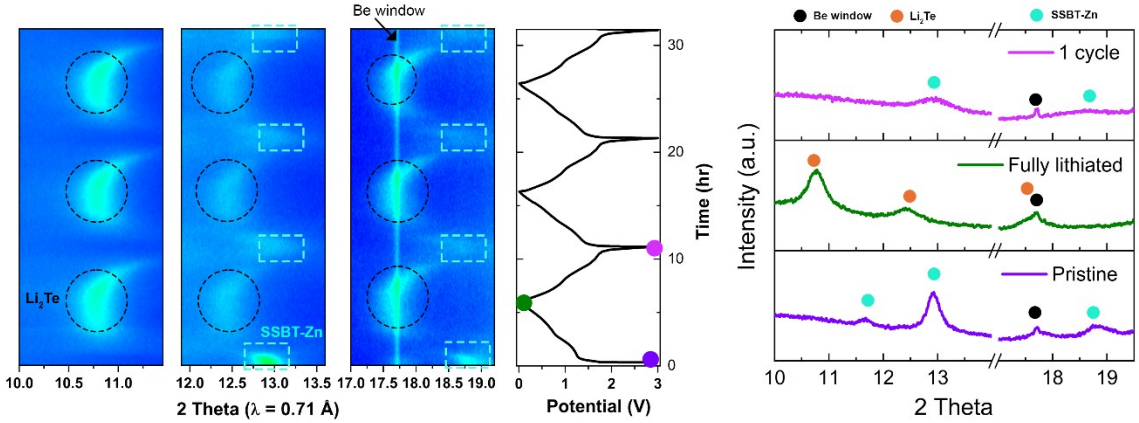

Fig. S14. *Operando* XRD of SSBT-Zn in lithium half-cell at C/5.